Mobility and diffusivity in a generalized Frenkel-Kontorova model

Oleg M. Braun

Institute of Physics, the Ukrainian National Academy of Sciences, 46 Science Avenue, UA-252022 Kiev, Ukraine
and Laboratoire de Physique, Ecole Normale Supérieure de Lyon, 46 Allée d'Italie, 69364 Lyon Cédex 07, France

Thierry Dauxois*

Laboratoire de Physique, Ecole Normale Supérieure de Lyon, 46 Allée d'Italie, 69364 Lyon Cédex 07, France

Maxim V. Paliy

Institute of Physics, the Ukrainian National Academy of Sciences, 46 Science Avenue, UA-252022 Kiev, Ukraine

Michel Peyrard

Laboratoire de Physique, Ecole Normale Supérieure de Lyon, 46 Allée d'Italie, 69364 Lyon Cédex 07, France
(Received 11 January 1996)

Molecular dynamics simulations are used to investigate the atomic mobility and diffusivity of a generalized Frenkel-Kontorova model which takes into account anharmonic (exponential) interaction of atoms subjected to a three-dimensional substrate potential periodic in two dimensions and nonconvex (Morse) in the third dimension. The numerical results are explained by a phenomenological theory which treats a system of strongly interacting atoms as a system of weakly interacting quasiparticles (kinks). Model parameters are chosen close to those for the K-W(112) adsorption system. [S0163-1829(96)00826-0]

I. INTRODUCTION

Experimental studies of transport coefficients in systems of strongly interacting atoms adsorbed on a crystalline surface show a very rich and complicated behavior, especially as functions of the atomic concentration. The variation of the diffusion coefficient versus coverage is particularly important for adsorbed layers where the concentration may vary in wide limits from zero (diffusion of isolated adsorbed atoms) to very high values (for example, in some adsystems the interatomic distance in a monolayer of adatoms is lower than that in the corresponding massive crystal).[1] The theoretical study of mass and charge transport in such systems is a very difficult problem; however, it was studied for various kinds of interactions by Gomer and co-workers[2] using Monte Carlo simulations. At high temperatures, transport coefficients can be found with a perturbation technique starting from the case of noninteracting atoms.[3] At low temperatures, the case of interacting atoms has been studied by a numerical calculation of the transport properties of the standard Frenkel-Kontorova (FK) model, which describes a chain of harmonically interacting atoms subjected to a one-dimensional sinusoidal external potential.[4,5] Recently, the low-temperature behavior of a system of strongly interacting atoms in a more general one-dimensional model has been approximately treated with a phenomenological approach which introduces weakly interacting quasiparticles.[6] This method provides analytical estimates for the transport coefficients, but it requires many approximations. In particular, the properties of the quasiparticles involved in the theory are deduced from results of the standard FK model, which provides only a simplified picture. Therefore it was necessary to check the validity of the theoretical approach by numerical simulations of a model which is sufficiently complicated to

provide a reasonable description of a real system. This is the aim of this paper, which studies a two-dimensional generalized FK model and also discusses some experimental results in the same perspective.

The original FK model was introduced to analyze the dynamics of dislocations in crystals[7] by considering a chain of interacting particles subjected to a periodic substrate (on-site) potential. It can describe, for example, a closely packed row of atoms in a crystal,[8] a chain of atoms adsorbed on stepped or furrowed crystal surfaces,[9] a chain of ions in a "channel" of a quasi-one-dimensional conductor,[10] hydrogen atoms in hydrogen-bonded systems,[11] etc. In all the cases mentioned above, the chain of interacting particles is an intrinsic part of the whole physical system under consideration. The role of the remainder of the system is played by an external substrate potential and a thermal bath. Although it is still oversimplified, the *generalized* FK model that we consider here provides a rather complete description of a layer of atoms adsorbed on a two-dimensional crystal surface. It includes realistic (exponential) interactions of particles instead of the harmonic springs of the standard FK model, and the substrate potential is three dimensional. It is periodic in the two dimensions parallel to the surface and has a Morse shape in the third direction, orthogonal to the surface.

The transport properties of the system are described by two coefficients, the mobility B and the chemical diffusivity D_c. The mobility defines the response of the system to an infinitesimal dc force F,

$$J = \rho B F, \tag{1}$$

where J is the atomic flux caused by the force and ρ is the average atomic concentration. On the other hand, the chemical diffusion coefficient D_c connects the flux $J(x,t)$ in a

nonequilibrium state to the gradient of the atomic concentration when $\rho(x,t)$ slightly deviates from its equilibrium value. According to Fick's law

$$\langle\langle J(x,t)\rangle\rangle \approx -D_c \frac{\partial}{\partial x}\langle\langle\rho(x,t)\rangle\rangle, \qquad (2)$$

where $\langle\langle\cdots\rangle\rangle$ stands for the averaging over macroscopic distances $x \gg a_A$, and a_A is the average interatomic distance. These two coefficients are coupled through the relation

$$D_c = \frac{k_B T B}{\chi}, \qquad (3)$$

where k_B is Boltzmann's constant, T the temperature, and χ the dimensionless susceptibility of the system.

The predictions of the phenomenological approach[6] can be summarized as follows. The mass transport is caused by kinks which describe localized compressions or expansions of the chain and therefore the mobility B can be expected to be proportional to the kink concentration. The kinks have two different origins, ''geometrical'' and thermal. We call geometrical kinks the kinks which result from the value of the coverage $\theta = N/M$, where N is the number of atoms and M the number of wells of the substrate potential on a given length. For $\theta = 1/q$, with integer q ($q = 1, 2, \ldots$), the system has a trivial ground state with one atom at the bottom of the substrate wells every qth well. When θ deviates slightly from such a value, the difference is accommodated by the system by forming localized discommensurations which are the geometrical kinks (called also ''trivial kinks'' in the notation of Ref. 6). As the kink density increases when θ deviates from $1/q$, the theory predicts that $B(\theta)$ should exhibit local minima for any trivial ground state (GS) of the system, such as $\theta = 1$, $\theta = 1/2$, $\theta = 1/3$, etc. When $\theta = p/q$ is a rational number with a larger numerator, such as $\theta = 2/3$, the density of geometrical kinks becomes very large and one could expect to get a high mobility B. The picture is, however, more complicated because, due to their high density, the geometrical kinks interact strongly and, when temperature is sufficiently low with respect to their interaction energy, they tend to form a regular lattice which is weakly pinned, giving a low mobility for any rational θ. A slight deviation from $\theta = p/q$ appears as discommensurations in the kink lattice, i.e., ''kinks in a kink lattice,'' which are called superkinks in Ref. 6. These topological excitations of the kink lattice contribute to mass transport exactly as the trivial kinks do, so that the mobility is expected to exhibit local minima for $\theta = p/q$ such as $\theta = 2/3$. In the limit $T \rightarrow 0$ the function $B(\theta)$ should therefore have minima at any rational θ. When temperature increases, the secondary minima disappear because the kink lattice ''melts'' and, moreover, thermal fluctuations create kink-antikink pairs which are thermally activated. Consequently, at high enough temperature the mobility is expected to exhibit broad maxima between the primary minima at $\theta = 1/q$. Such a behavior has been observed in one-dimensional models.[12–14]

The behavior of the diffusion coefficient D_c is simpler than the variation of $B(\theta)$ as predicted in Ref. 15. According to Fick's law (2), D_c is the proportionality coefficient between the (infinitesimal) gradient of the atomic concentration and the flux of atoms caused by this gradient. However, a gradient of atomic concentration automatically produces a corresponding gradient of kink concentration. In the standard FK model, where the elastic constant does not depend on θ and where the parameters of kinks and antikinks are the same, $D_c(\theta)$ is the ratio of two quantities which vary similarly so that it should be approximately constant and coincide with the kink (or antikink) diffusion coefficient. In the generalized FK model the situation is different because the anharmonicity of the interatomic interaction destroys the kink-antikink symmetry.[16] The effective interatomic forces for a kink, which corresponds to a local contraction of the chain, exceed those for an antikink, which is associated with a region of a local extension. Thus, in comparison with an antikink, a kink is characterized by a larger value of the rest energy and by lower values of effective mass and activation energy for its motion.[15] When the coverage passes through a commensurate value θ_0, the geometrical-kink density vanishes; for $\theta < \theta_0$ the system has geometrical antikinks while for $\theta > \theta_0$ the system has geometrical kinks. Therefore, when the coverage θ increases through a commensurate value θ_0, the activation energy for the chemical diffusion should jump to a smaller value. Simultaneously, the value of D_c should rise sharply when the coverage θ exceeds the value θ_0 that characterizes a ''well-defined'' commensurate structure and one could expect $D_c(\theta)$ to exhibit the shape of a devil's staircase. The abrupt (jumplike) increase of $D_c(\theta)$ will only exist in the $T \rightarrow 0$ limit and, for any $T \neq 0$, these jumps will be smoothed owing to corrections from thermally excited kink-antikink pairs.

In the present paper we check these predictions by molecular dynamics investigations of the low-temperature mobility and diffusivity of a generalized FK model in one and two dimensions. In Sec. II, we describe the model and define its parameters. Kink parameters are calculated in Sec. III. Simulation results for the mobility are presented in Sec. IV, and those for the chemical diffusivity are described in Sec. V. Section VI discusses known experimental results in the framework of these studies and Sec. VII concludes the paper.

II. THE MODEL

As for the standard FK model, we consider the dynamics of atoms adsorbed on a periodic substrate. The displacement of each atom is characterized by three variables: x and y describe its motion parallel to the surface, while z describes its deviation orthogonal to the substrate. For the substrate potential, we take the function

$$V_{\text{sub}}(x,y,z) = [V_{\text{pr}}(x;a_{sx},\varepsilon_{sx},s_x) + V_{\text{pr}}(y;a_{sy},\varepsilon_{sy},s_y)]e^{-\gamma' z}$$
$$+ V_z(z). \qquad (4)$$

To model the substrate potential along the surface, we use a deformable periodic potential which can be adjusted to describe an actual crystal field,[17]

$$V_{\text{pr}}(x;a_{sx},\varepsilon_{sx},s_x) = \frac{\varepsilon_{sx}}{2}\frac{(1+s_x)^2[1-\cos(2\pi x/a_{sx})]}{1+s_x^2-2s_x\cos(2\pi x/a_{sx})}. \qquad (5)$$

Thus ε_{sx} corresponds to the activation energy for diffusion of a single atom along the x direction, a_{sx} to the lattice

constant, and the parameter s_x ($|s_x| < 1$) controls the shape of the substrate potential. The frequency ω_x of a single-atom vibration along the x direction is connected to the shape parameter s_x by the relationship $\omega_x = \omega_0 (1 + s_x)/(1 - s_x)$, where $\omega_0 \equiv (\varepsilon_{sx}/2m)^{1/2} (2\pi/a_{sx})$ and m is the atomic mass. The potential $V_{pr}(y; a_{sy}, \varepsilon_{sy}, s_y)$ has the same form.

The potential perpendicular to the surface is modeled by the Morse function

$$V_z(z) = \varepsilon_d (e^{-\gamma z} - 1)^2, \qquad (6)$$

which tends to the adsorption energy ε_d when z goes to infinity. The anharmonicity parameter γ is related to the frequency ω_z of a single-atom vibration in the normal direction by the relation $\omega_z^2 = 2\gamma^2 \varepsilon_d/m$.

Finally, the exponential factor after the square brackets of the right-hand side of Eq. (4) takes into account the decrease of the influence of the surface corrugation as the atoms move away from the surface, so that $V_{sub}(x, y, z) \to \varepsilon_d$ when $z \to \infty$.

For the interaction between the atoms we take the exponential repulsion

$$V_{int}(r) = V_0 \exp(-\beta_0 r), \qquad (7)$$

where V_0 is the amplitude and β_0^{-1} determines the typical range of the interaction. This potential is adapted to describe rather high coverages such that the atoms interact through the repulsive branch of the interatomic potential. In numerical simulations, we can only include the interaction of a given adatom with a finite number of neighbors. Therefore we use the standard approach of molecular dynamics (MD) simulations and introduce a cutoff distance r^*. We account only for the interactions between the atoms separated by distances lower than r^*, and to reduce errors caused by this procedure the interaction potential (7) is truncated as

$$\widetilde{V}_{int}(r) = V_{int}(r) - V_{int}(r^*) - V'_{int}(r^*)(r - r^*), \qquad (8)$$

so that the interaction potential and force vanish at the cutoff distance, $\widetilde{V}_{int}(r^*) = \widetilde{V}'_{int}(r^*) = 0$ (the tilde will be omitted in what follows). In addition, because we are using the repulsive interatomic interaction, we have to fix the atomic concentration. It is imposed by periodic boundary conditions in x and y. We place N atoms in the fixed area $L_x \times L_y$, $L_x = M_x a_{sx}$, $L_y = M_y a_{sy}$, so that the dimensionless atomic concentration is equal to $\theta = N/M$, where $M = M_x M_y$.

To model the energy exchange of the atoms with a thermal bath, we use the Langevin equations for atomic coordinates x_i,

$$m\ddot{x}_i + m\eta\dot{x}_i + \frac{d}{dx_i}\left[V_{sub}(x_i, y_i, z_i) + \sum_{j \neq i} V_{int}(|\vec{r}_i - \vec{r}_j|) \right]$$
$$= F^{(x)} + \delta F_i^{(x)}(t), \qquad (9)$$

and similar equations for y_i and z_i. Here, η corresponds to the rate of the energy exchange with the substrate, $\vec{F} = \{F, 0, 0\}$ to the dc driving force, and δF is a Gaussian random force with correlation function

$$\langle \delta F_i^{(\alpha)}(t) \delta F_j^{(\beta)}(t') \rangle = 2\eta m k_B T \delta_{\alpha\beta} \delta_{ij} \delta(t - t'). \qquad (10)$$

We use a dimensional system of units adapted to the scales of the problem. Distance is measured in angströms, energy and temperature in eV. The mass of an adatom is chosen as our mass unit ($m = 1$). This imposes a time scale. We measure time in units of the characteristic time interval $t_0 = 2\pi/\omega_x$. In the remainder of the paper, the measures of other dimensional physical quantities will be omitted, but they are all expressed in terms of the above-defined units.

In order to be close to real physical systems, let us take the adsystem K-W(112) as an example to define the model parameters: the W(112) surface is characterized by a strong anisotropy of the atomic relief because it has close-packed rows of substrate atoms separated by furrows of atomic depth. Namely, in the simulation, we put $a_{sx} = 2.74$ Å and $a_{sy} = 4.47$ Å, which are, respectively, the distances between the neighboring wells along and across the furrows on the W(112) surface, and $\varepsilon_{sx} = 0.46$ eV and $\varepsilon_{sy} = 0.76$ eV for the corresponding barriers (these values were taken from Ref. 18). To model the shape of the substrate potential, we have to define the parameters s_x and s_y. They can be estimated to be within the range [0.2,0.4].[19] For the sake of concreteness we took $s_x = 0.2$ and $s_y = 0.4$, which leads to the following frequencies of adatom vibrations: $\omega_x = 1.65$ and $\omega_y = 2.02$. The experimental value for the adsorption energy of K on W is $\varepsilon_d = 2.54$ eV.[18] For the vibration frequency normal to the surface we took $\omega_z = \frac{1}{2}(\omega_x + \omega_y) = 1.84$, which gives $\gamma = 0.813$. For the interatomic potential (7), we took the parameters $V_0 = 10$ eV and $\beta_0 = 0.85$ Å^{-1}. These choices give reasonable values for adsystems:[20] the interaction energies between two adatoms occupying the nearest wells along the furrow and across are equal to $V_{int}(a_{sx}) \approx 0.98$ eV and $V_{int}(a_{sy}) \approx 0.22$ eV, respectively. Finally, we have to define the rate of energy exchange between the adatoms and substrate: we took the typical value[21] $\eta = 0.1\omega_x = 0.165$. Note that although some of the parameters are chosen rather arbitrarily, they are typical for metal atoms adsorbed on metal substrates.[22] However, as the model is still oversimplified to describe a real adsystem, we have to say that our choice of parameters does not claim to provide a quantitative interpretation of the K-W(112) adsystem. We do nevertheless believe in the qualitative description of the effects under investigation and claim that typical adsystems on anisotropic surfaces [e.g., lithium and strontium on the molybdenum (112) surface, for which experimental data on the detailed coverage dependencies of diffusion characteristics are available[23]] should exhibit a similar behavior. Finally, for numerical solution of the Langevin equations (9), we use the standard fourth-order Runge-Kutta method with the time step $\Delta t = t_0/20 = 0.19$, and the cutoff radius was taken as $r^* = 2a_{sy} = 8.94$ Å .

III. KINKS

As the kinks are the main objects of the phenomenological approach,[6] let us first calculate their parameters. We recall that kinks can be defined for any commensurate atomic structure $\theta_0 = s/q$, where s and q are relative prime integers; the kink (antikink) describes then the minimally possible topologically stable compression (expansion) of the commensurate structure. The kink is a quasiparticle, characterized by an effective mass m_k, a rest energy ε_k, and the Peierls-

Nabarro (PN) amplitude ε_{PN}, corresponding to the barrier for the kink translation along the chain. These parameters are determined by the dimensionless elastic constant g_{eff} defined as

$$g_{eff} = \frac{a_{sx}^2}{2\pi^2\varepsilon_{sx}} V''_{int}(a_A). \qquad (11)$$

Analytically, the kink parameters may be found in the low-coupling limit $g_{eff} \ll 1$ or in the strong-coupling (sine-Gordon) limit[6] $g_{eff} \gg 1$; however, the usual real physical systems are characterized by the elastic constant $g_{eff} \sim 1$, so that both approximations are too crude to be applied to our case. For our choice of model parameters, we have $g_{eff} \approx 0.6$ for $\theta_0 = 1$. Therefore we will calculate the kink parameters numerically.

The numerical method was described in detail in previous papers.[15,24] Briefly, we have to choose first an appropriate size of the finite chain in order to insert a single kink into the $\theta_0 = s/q$ commensurate background structure; the integers N and M must satisfy the equation[15,25]

$$qN = sM + \sigma, \qquad (12)$$

where the kink topological charge σ is equal to $\sigma = +1$ for the kink and $\sigma = -1$ for the antikink. In the simulation, we restrict ourselves to the concentration range $[0.5, 1]$ because for lower concentrations the interatomic interaction is too weak and its effects would be hardly observable, while at higher concentrations the atoms begin to escape from the first adlayer.[24,26] As background structures, we chose the following coverages: $\theta_0 = 1/2$, $\theta_0 = 3/5$, $\theta_0 = 2/3$, $\theta_0 = 3/4$, $\theta_0 = 4/5$, and $\theta_0 = 1$. The corresponding values for the number of atoms N_0 and the number of minima of the substrate potential M_0 for every θ_0 are summarized in Table I.

We start with an appropriate initial configuration and allow the atoms to reach the minimum energy configuration (see details in Refs. 26 and 27). This determines the structure of a kink in its minimal energy state. Then, in order to calculate the parameters that characterize the kink translation, we choose a given atom in the kink region (see Ref. 15) and move it to the right by small steps by imposing its x coordinate while all other degrees of freedom of the chain remain free to adjust to every new position of the constrained atom. This process allows us to find the saddle configuration and therefore the amplitude of the PN barrier ε_{PN} as the difference of the saddle and GS energies. In addition, the energy of creation of the kink-antikink pair is determined as $\varepsilon_{pair} = E\{kink[\theta_0]\} + E\{antikink[\theta_0]\} - 2E\{GS[\theta_0]\}$, where $E\{\cdot\}$ is the energy of the corresponding configuration (notice that it must satisfy the relation $N\{kink[\theta_0]\} + N\{antikink[\theta_0]\} = 2N\{GS[\theta_0]\}$ which is imposed by the total length of the atomic chains along x). The kink parameters obtained by this method are summarized in Table I, and the dependence of the PN energy on the atomic concentration is presented in Fig. 1. Note that the function $\varepsilon_{PN}(\theta)$ has the shape of a devil's staircase.[15]

From the kink parameters, the phenomenological approach[6] describes approximately the low-temperature behavior of the system as follows. For $\theta = 1$ and

TABLE I. Parameters of kinks: N_0 is the number of atoms, M_0 the number of minima of the substrate potential for one period of the system along x, ε_{pair} the creation energy of a kink-antikink pair, and ε_{PN} the amplitude of the Peierls-Nabarro potential.

Structure	N_0	M_0	ε_{pair} (eV)	ε_{PN} (eV)
Antikink[1/2]	21	43		0.378
$\theta_0 = 1/2$	21	42	0.759	
Kink[1/2]	21	41		0.0849
Antikink[3/5]	22	37		0.0848
$\theta_0 = 3/5$	21	35	0.007	
Kink[3/5]	20	33		0.0813
Antikink[2/3]	21	32		0.0812
$\theta_0 = 2/3$	20	30	0.170	
Kink[2/3]	21	31		0.0192
Antikink[3/4]	20	27		0.0184
$\theta_0 = 3/4$	21	28	0.055	
Kink[3/4]	22	29		0.0087
Antikink[4/5]	19	24		0.0086
$\theta_0 = 4/5$	20	25	0.018	
Kink[4/5]	21	26		0.0071
Antikink[1]	21	22		0.0071

$T \ll \varepsilon_{pair}\{\theta_0\}/k_B$ the concentration of thermally nucleated kink-antikink pairs is equal to[28–32]

$$\langle \theta_{pair} \rangle \approx C \exp(-\epsilon_{pair}/2k_BT), \qquad (13)$$

where $C \approx (2\tilde{m}_k \omega_x^2 a_{sx}^2 / \pi k_B T)^{1/2}$ and $\tilde{m}_k = (m_k m_{\bar{k}})^{1/2}$. For lower coverages $\theta = \theta_0 = s/q$ Eq. (13) should be properly renormalized, which results in an additional factor $1/q$ in its right-hand side.
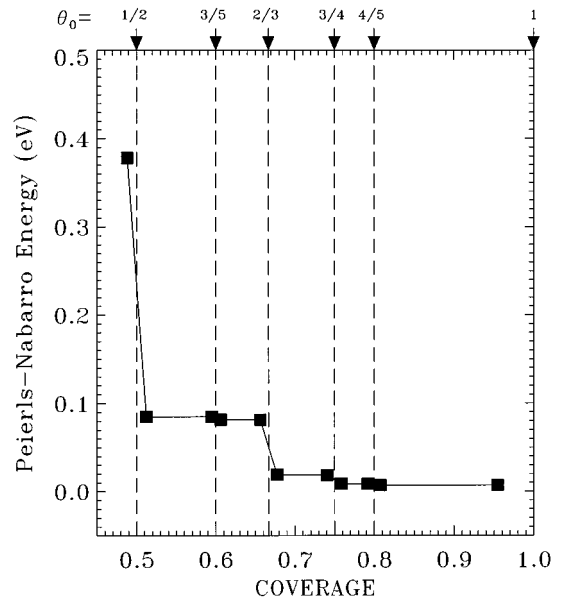

FIG. 1. Peierls-Nabarro energy versus coverage. Coverages corresponding to simplest commensurate structures are shown with dashed lines.

When the concentration θ slightly deviates from the commensurate value θ_0, the thermal kinks are supplemented by geometrical kinks (if $\theta > \theta_0$) or antikinks (if $\theta < \theta_0$) with a concentration $\theta_{geom} = q|\theta - \theta_0|$. In the close vicinity of θ_0, the total kink concentration can be found as

$$\langle \theta_{tot} \rangle \approx \theta_{geom} + 2 \langle \theta_{pair} \rangle. \tag{14}$$

The dimensionless susceptibility χ

$$\chi = \langle \theta_{tot} \rangle / q^2 \theta \tag{15}$$

can then easily be obtained from Eqs. (13) and (14).

Let us now examine the phenomenology of subsequently melted kink superlattices.[6] In order to describe the atomic mobility in terms of collective excitations, we must first define the type of excitations that have to be considered. As an example, let us select a concentration θ in the neighborhood of $\theta_0 = 2/3$. For low T, $T < \varepsilon_{pair}\{2/3\}/2k_B$, we have to use the superkinks defined on the background of the $\theta_0 = 2/3$ structure in the expressions (13)–(15). However, in the intermediate temperature range, i.e., $\varepsilon_{pair}\{2/3\}/2k_B < T < \varepsilon_{pair}\{1/2\}/2k_B$, when the superkinks are destroyed by thermal fluctuations while the trivial kinks (defined on the $\theta_0 = 1/2$ background) are not yet destroyed, we have to substitute the parameters of the trivial kinks in Eqs. (13) and (14). In particular, we should take $q = 3$ for low T but $q = 2$ for intermediate temperatures. In the latter case, however, the parameters of trivial kinks may seriously differ from those calculated for the ideal case, because the concentration of trivial kinks at the $\theta = 2/3$ coverage is very large and their interaction is not negligible.

When the amplitude of the activation barrier for the kink motion is known, the diffusion coefficient D_k for a single-kink random walk may be approximately calculated with the Kramers theory. For $T < \varepsilon_{PN}/k_B$ this approach gives

$$D_k = D_{k0} \exp(-\varepsilon_{PN}/k_B T), \tag{16}$$

where

$$D_{k0} \approx \begin{cases} a^2 \omega_{PN}/2\pi & \text{if } \eta_l < \eta < \omega_{PN}, \\ a^2 \omega_{PN}^2/2\pi\eta & \text{if } \eta > \omega_{PN}. \end{cases} \tag{17}$$

Here $\omega_{PN} \approx (\pi/a_{sx})(2\varepsilon_{PN}/m)^{1/2}$, $a = q a_{sx}$, and $\eta_l = \omega_{PN} k_B T/2\pi\varepsilon_{PN}$.

If the interatomic interaction is strong enough, the inequality $\varepsilon_{PN} < \varepsilon_{pair}$ may easily be fulfilled. In this case, within the temperature interval $\varepsilon_{PN} < k_B T < \varepsilon_{pair}$, the kink diffusion coefficient is approximately equal to (e.g., see Refs. 33–35)

$$D_k \approx \frac{k_B T}{m_k \eta} \left[1 - \frac{1}{8} \left(\frac{\varepsilon_{PN}}{k_B T} \right)^2 \right]. \tag{18}$$

Knowing the kink diffusion coefficient, we can find the chemical diffusion coefficient with the phenomenological approach[6] by the formula

$$D_c \approx \frac{\langle \theta_k \rangle D_k + \langle \theta_{\bar{k}} \rangle D_{\bar{k}}}{\langle \theta_{tot} \rangle}, \tag{19}$$

where for $\theta > \theta_0$ we should take $\langle \theta_k \rangle = \theta_{geom} + \langle \theta_{pair} \rangle$ and $\langle \theta_{\bar{k}} \rangle = \langle \theta_{pair} \rangle$, while in the $\theta < \theta_0$ case, we have to substitute

$\langle \theta_k \rangle = \langle \theta_{pair} \rangle$ and $\langle \theta_{\bar{k}} \rangle = \theta_{geom} + \langle \theta_{pair} \rangle$. Finally, the chain mobility may be found as $B = \chi D_c$. These predictions should be now compared with the results of simulation and this is the subject of the following section.

IV. MOBILITY

To study the mobility, we use an algorithm where we look first for the minimum energy configuration of the system. Then we increase the temperature up to a given temperature T by small steps $\Delta T = T/50$ during the time $t_{therm} = 100 t_0 = 381$. At that point, we apply a small dc force $F = 0.01$ which is gradually increased from $F = 0$ to $F = 0.01$ during the time $100 t_0$, and wait during $t_{wait} = 100 t_0$ in order to allow the system to reach a stationary state. Then, for the discrete times $t_n = n t_0$, we measure the average velocity $\langle v_x \rangle$ of the atoms during $t_{run} = 100 t_0$, and, finally, the procedure is repeated n_{av} times ($n_{av} = 5$ in the simulation) with different initializations of the random number generator in order to estimate the error bars.

To demonstrate the effect of the transverse degrees of freedom on the atomic mobility, we considered three different cases of the generalized Frenkel-Kontorova model:

(i) a purely one-dimensional atomic chain with atomic movement restricted to the x direction (1D);

(ii) a quasi-one-dimensional atomic chain with two transverse degrees of freedom y and z (we will call it the quasi-1D case);

(iii) a true two-dimensional extension of the FK model (2D).

Note that the interaction between the atoms always has the general form of Eq. (7), i.e., it has a 3D character in the quasi-1D and 2D cases.

The quasi-1D case can be easily obtained from the general case by choosing a period of one lattice constant in the y direction; namely, we put $M_y = 1$ so that all chains move in the same way and chose $N = 5 N_0 \{\theta\}$ and $M_x = 5 M_0 \{\theta\}$, where the integers N_0 and M_0 are taken from Table I for each coverage θ in order to have five kinks or antikinks over the length under investigation. The results of the simulations are presented in Fig. 2. As expected from the phenomenological theory, at low temperatures $B(\theta)$ does have local minima not only for the trivial concentrations $\theta = 1/2$ and $\theta = 1$, but also at the commensurate concentrations $\theta = 2/3$ and $\theta = 3/4$. These two minima, which involve a kink lattice, disappear when the temperature is increased, while the minima for the trivial structures survive at any temperature. In the simulation, minima do not appear for the other complicated GS structures (e.g., $\theta = 3/5$ and $\theta = 4/5$) because these higher-order structures correspond to too low "melting" temperatures of the kink lattice.

In order to check completely the phenomenological theory,[6] it would be interesting to see if these extra minima appear at very low temperature, but the mobility is then too small to allow us to obtain accurate results in a numerical simulation. As the "melting" temperature is determined by the magnitude of the effective elastic constant of the kink lattice, one could attempt to increase the parameter V_0 in Eq. (7). But in that case, the repulsion between the atoms is too large and they begin to escape from the minima of the substrate potential in the direction orthogonal to the chain.[27] To
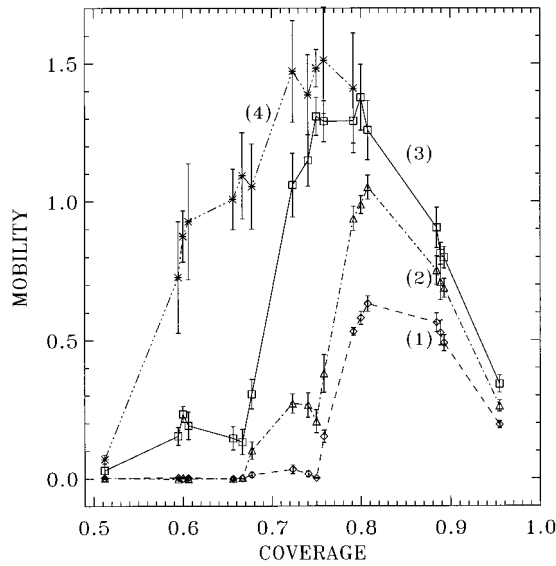
perature is increased, while the minimum at $\theta = 2/3$ survives in the whole range of investigated temperatures, since it has a greater melting temperature. However, the minima at $\theta = 3/5$ and $\theta = 4/5$, where the kink lattice has the period $5a_{sx}$, are not found even for this very strong interatomic repulsion. Note also that in real physical systems, such as adsorbed layers, the observation of local minima for these complicated structures is unlikely due to the existence of transverse degrees of freedom.

In a one-dimensional model at high enough temperature ($T > \varepsilon_{pair}/k_B$), the mobility can be calculated with a perturbative approach starting from a system of noninteracting atoms. The function $B(\theta)$ is given by[12–14]

$$B \approx B_f \left\{ 1 + \frac{1}{8} \left[\frac{(\varepsilon_{sx}/k_B T) \sinh(k_B T/\varepsilon_{sx} g_A)}{\cosh(k_B T/\varepsilon_{sx} g_A) - \cos(2\pi a_A/a_{sx})} \right]^2 \right\}^{-1},$$

$$(20)$$

where $B_f = 1/m\eta$, $a_A = a_{sx}/\theta$ is the average interatomic distance, and the elastic constant g_A is defined by $g_A = a_{sx}^2 V''_{int}(a_A)/2\pi^2 \varepsilon_{sx}$. Note that the function (20) has local minima for trivial configurations only, in agreement with the phenomenological theory in the high-temperature range. The chemical diffusivity D_c could be obtained by replacing the prefactor B_f in Eq. (20) by $a_A^2 V''_{int}(a_A)/m\eta$. Figure 3 shows that Eq. (20) describes the high-temperature simulation results of the purely one-dimensional FK model with good accuracy (except in the vicinity of the coverage $\theta = 2/3$, where $\varepsilon_{pair}/k_B > T$ even for the highest studied temperature). For this model, the highest possible mobility $B_f = 1/m\eta \approx 6.0$, which corresponds to the case of noninteracting free atoms, is reached in the middle of the interval $0.5 < \theta < 1.0$.

The high-temperature mobility for the quasi-1D chain with transverse degrees of freedom [curve (4) in Fig. 2] is approximately two times lower than the values calculated with Eq. (20) for corresponding parameters. Note that, for the chosen set of parameters in a quasi-1D model, $T = 0.05$ eV is the highest temperature for which the determination of the mobility *in the first monolayer of atoms* is possible. At higher temperatures the atoms start to escape from the first layer to the second one, which may seriously distort the results [the curve (4) in Fig. 2 is not plotted at $\theta > 0.8$ for this reason]. Even if one takes into account the fact that the high-temperature range required for the validity of Eq. (20) is not reached, the disagreement between Eq. (20) and the simulation results is large in the quasi-1D case. This shows that the presence of the transverse degrees of freedom has the same effect on the mobility as an additional friction in the system. This can be understood because some part of the work done by the external force is used to excite the transverse degrees of freedom.

Finally, we also simulated the 2D Frenkel-Kontorova system with $M_y = 30$, $M_x = M_0\{\theta\}$, and $N = 30 N_0\{\theta\}$. The results, presented in Fig. 4, show that there is no essential difference between the $B(\theta)$ dependencies for the quasi-1D and 2D systems except that 2D dependencies are systematically lower. The role of the transverse degrees of freedom, already noticed for the quasi-1D model, show up again here. It is interesting to notice that Fig. 4 shows for the 2D model at $T \leq 0.01$ eV the additional small minimum of $B(\theta)$ at

FIG. 2. The mobility B of the quasi-1D FK model with transverse degrees of freedom as a function of the coverage θ at selected temperatures $T = 0.0025$ eV [curve (1)], $T = 0.005$ eV (2), $T = 0.020$ eV (3), and $T = 0.050$ eV (4).

prevent this escape and allow the study of higher-order minima, we artificially restricted the atomic displacements to the x dimension. This allowed us to take $V_0 = 100$ eV. This case corresponds to the so-called 1D case. The results are shown on Fig. 3.

As seen from Fig. 3, in the 1D case the function $B(\theta)$ has pronounced local minima at $\theta = 2/3$ and $\theta = 3/4$ at much higher temperatures than in the quasi-1D case. One can note also that the minimum at $\theta = 3/4$ disappears when the tem-
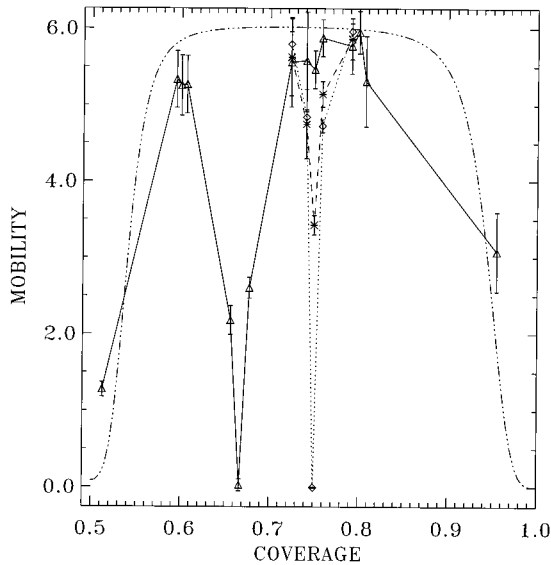

FIG. 3. The mobility B versus coverage θ for a purely 1D model with $V_0 = 100$ eV at different temperatures $T = 0.005$ eV (diamonds and dotted line), $T = 0.05$ eV (asterisks and dashed line), and $T = 0.10$ eV (triangles and solid line). For a better presentation, the data for the two lower temperatures are plotted only within $0.72 < \theta < 0.8$, because at other coverages they are the same as for $T = 0.10$ eV. The dash-triple-dotted line is Eq. (20) for $T = 0.10$ eV.
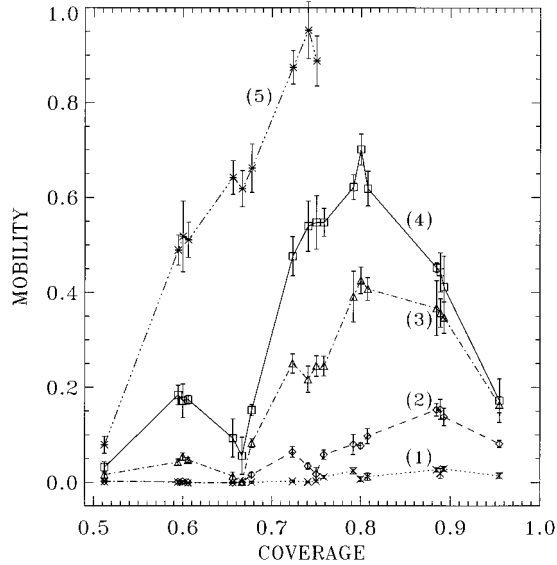
FIG. 4. The mobility B versus coverage θ for a 2D model at selected temperatures $T=0.005$ eV [curve (1)], $T=0.010$ eV (2), $T=0.020$ eV (3), $T=0.030$ eV (4), and $T=0.050$ eV (5).

$\theta=4/5$ predicted by the phenomenological theory, which reflects the existence of the kinks/antikinks on the background of this coverage.

The plots of the mobility B versus inverse temperature shown in Fig. 5 for the 2D model at selected coverages show that the atomic mobility has an activated character in the investigated range of temperatures and coverages. The same qualitative behavior was found for the 1D case. Using an Arrhenius form $B(T)=B_0 \exp(-E_a/T)$, we can calculate the activation energy E_a and the prefactor B_0. Their dependence on coverage is shown in Fig. 6. The activation energy E_a has a sharp maximum at the coverage $\theta=2/3$, which corresponds to a well-defined commensurate structure, while activation barriers on both sides of $\theta=2/3$ are much lower due to the presence of residual kinks/antikinks; the barrier for "kink" coverage $\theta=2/3+\delta$ is lower than that for "antikink" coverage $\theta=2/3-\delta$. On the other hand, the maxima of E_a at the higher-order commensurabilities $\theta=3/4$ and $\theta=4/5$ are much less pronounced. This is consistent with the fact that these higher-order commensurabilities hardly show up in the mobility curves of Fig. 4.

The main difference between the quasi-1D system and the true 2D model is due to the interactions of kinks in the nearest neighboring channels. For the repulsive interatomic interaction studied in the present work, kinks in the nearest neighboring channels repel each other at the $\theta=1$ coverage, while for any $\theta<1$ they attract each other and tend to form domain walls. With the short-range (exponential) interaction studied in our simulations, two kinks belonging to neighboring channels attract each other with a potential $V_{kk}(x)\propto|x|$, contrary to the usual law[9] $V_{kk}(x)\propto x^2$. As a consequence, the stiffness of the domain walls vanishes and they can be destroyed by thermal fluctuations or external forces for any $T\neq 0$ or $F\neq 0$. This is confirmed by the observation of snapshots of the atomic configuration in the 2D model. During the time evolution a domain wall of kinks is destroyed as soon as the temperature is high enough to provide a noticeable value of the mobility. For example, Fig. 7 demonstrates the evolution of such a domain wall defined on the background of the $\theta=1/2$ commensurate structure. This case was chosen because its kinks have the simplest structure and are more visible than kinks defined on the background of any other more complex commensurate structure. The initially well-defined kink wall (relaxed configuration for $T=0$) is smeared out at $T=0.02$ eV and $F=0.01$, although these values of temperature and external force provide a very low value of the atomic mobility ($B\approx 0.03$) at the chosen coverage. This instability of the kink domain walls explains why the true 2D model gives results which are not fundamentally different from the results of the quasi-1D case. Nevertheless, the interaction between atoms and kinks in the nearest neighbor channels does contribute to the dynamics of the system. It results, in particular, in the lowered values of mobility for the 2D case in comparison with those for a 1D system. However, in more realistic 2D models with long-range interatomic forces such as elastic or dipole-dipole forces due to the substrate, the role of the domain walls might be more essential.

V. DIFFUSION

The chemical diffusion coefficient is more difficult to calculate by MD simulations than the mobility. It can be determined in two ways. First, the susceptibility χ can be calculated with one of the methods described in Ref. 5 and then D_c could be derived from the relation $D_c=B/\chi$. However, this approach relies on the accuracy of the two factors. In the present work, we use a direct approach based on the Fick law (2). We start from a nonuniform initial concentration profile $\theta(x)$ and observe its evolution with time at a given temperature T (we will now use the notation θ instead of $\langle\langle\rho\rangle\rangle$ in the diffusion laws, assuming the existence of local equilibrium). The variations of the chemical diffusion coefficient D_c with concentration determine the diffusion profile.[1] For instance, for an approximately constant flux $J=-D_c \partial\theta/\partial x$, flat sections of the observed concentration profile (low $\partial\theta/\partial x$) correspond to enhanced diffusivity D_c, while sharp changes of concentration within some concentration interval (high
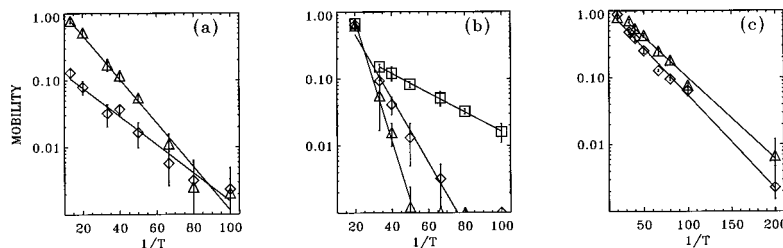

FIG. 5. The mobility B of the two-dimensional model versus the inverse temperature: (a) for coverages $\theta=0.51$ (diamonds) and $\theta=0.60$ (triangles); (b) kinks (squares), antikinks (diamonds), and the background commensurate structure (triangles) for $\theta_0=2/3$; (c) for coverages $\theta=0.72$ (diamonds) and $\theta=0.80$ (triangles).
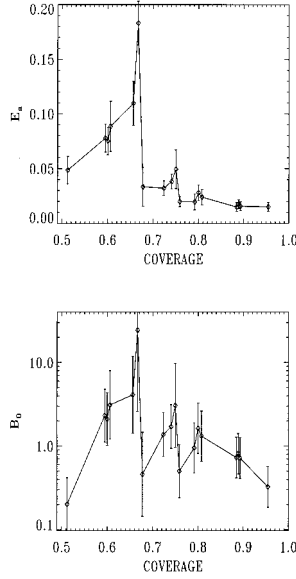
FIG. 6. The activation energy E_a and prefactor B_0 for the mobility versus coverage θ in the case of the two-dimensional FK model.
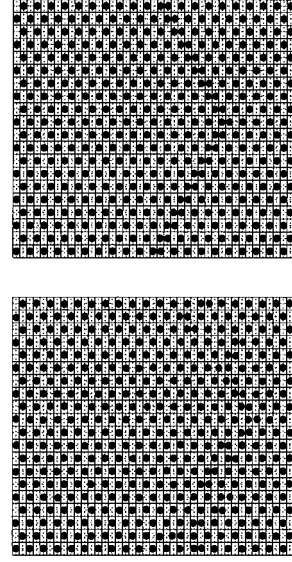

FIG. 7. Snapshot pictures for two-dimensional model at $\theta = 0.51$. (Top) The initial relaxed configuration ($T=0$) and (bottom) the atomic configuration after the evolution time $t \approx 1600$ at $T = 0.02$ eV.

$\partial \theta / \partial x$) indicate a lower diffusion coefficient D_c.

Quantitative data on the variation versus θ of the diffusion coefficient D_c can be obtained by studying the concentration profiles given by the one-dimensional diffusion equation

$$\frac{\partial}{\partial t} \theta(x,t) = \frac{\partial}{\partial x} \left(D_c(\theta) \frac{\partial \theta(x,t)}{\partial x} \right). \qquad (21)$$

The simplest case is the diffusion of an initially stepwise profile in a spatially infinite system, which gives an explicit expression for the $D_c(\theta)$ function by the Boltzmann-Matano formula (see, e.g., Ref. 1). However, with periodic boundary conditions, computational limitations do not allow us to choose a period large enough to observe such a profile. Therefore we first derive an approximate expression of $D_c(\theta)$ using the phenomenological equations (13)–(19), and then solve Eq. (21) with this $D_c(\theta)$ and periodic boundary conditions. Finally, we compare the calculated profiles with those obtained from MD simulation for the same initial distribution.

Let us first apply the kink-gas phenomenology to the determination of D_c. We have chosen the room temperature $T = 0.025$ eV (290 K) since it divides the whole investigated coverage interval [0.5,1.0] into two parts which differ by the mechanism of kink diffusion. For the coverage range $0.5 < \theta < 0.66$ where the condition $T < \varepsilon_{PN}/k_B$ is satisfied (see Fig. 1), the diffusion of kinks has an *activated* character and, in terms of the Arrhenius representation of the chemical diffusion coefficient $D_c = D_0 \exp(-E_{ac}/T)$, this means that the $D_c(\theta)$ dependence is determined mainly by the variations of the activation energy [note that $E_{ac} \approx \varepsilon_{PN}$ according to Eq. (16)]. On the other hand, for $0.66 < \theta < 1.0$, where $T > \varepsilon_{PN}/k_B$ and where the Peierls-Nabarro energy ε_{PN} shows only minor changes with coverage, the mass transport is car-

ried out by *free* diffusion of kinks and the main variations of chemical diffusion coefficient will arise from the prefactor D_0.

One should keep in mind that the phenomenological equations (13)–(19) can be used only for those kinks which are well defined as quasiparticles for a given temperature and a given coverage interval, i.e., the condition $T \ll \varepsilon_{pair}/k_B$ must be satisfied. In other words, the concentration of thermally excited kink/antikink pairs (13) for a given structure $\theta_0 = s/q$ cannot exceed the maximal possible value $1/q$. For the present study, it means that the quasiparticles which should be taken into account at $T = 0.025$ eV are the trivial kinks/antikinks of the trivial GS $\theta_0 = 1/2$ and $\theta_0 = 1$ and superkinks defined on the background of $\theta_0 = 2/3$ structure. We pointed out in Sec. III that, for our model parameters, accurate kink parameters can only be determined numerically. But in order to solve Eq. (21) we need some expression for the kink masses. Since the maximum value of the dimensionless elastic constant g_{eff} defined by Eq. (11) approximately equals 0.6 for the chosen set of model parameters, the best estimate is given by the low-coupling-limit expression[6] $m_k \approx m_{\bar{k}} \approx m/q^2$.

Theoretically, the application of the Eqs. (13)–(19) for the determination of D_c is only strictly valid in the close vicinity of commensurate structures, where the concentration of residual kinks is low (in our case, near the coverages $\theta_0 = 1/2$, $\theta_0 = 2/3$, and $\theta_0 = 1$). Since we need $D_c(\theta)$ for all intermediate θ values, we have to interpolate between these specific θ values. We calculated the values of D_c (indicated by the plus signs in Fig. 8) up to the middle points between these specific coverages and used a weighting coefficient, plotted them in the inset in Fig. 8, to mark the significance of each point in the subsequent interpolation procedure. The final form of $D_c(\theta)$ is taken as a superposition of $\tanh(\theta)$ functions chosen to provide a good fit of the value deduced from the phenomenological theory around the coverages $\theta_0 = 1/2$, $\theta_0 = 2/3$, and $\theta_0 = 1$, where it is accurate. Although
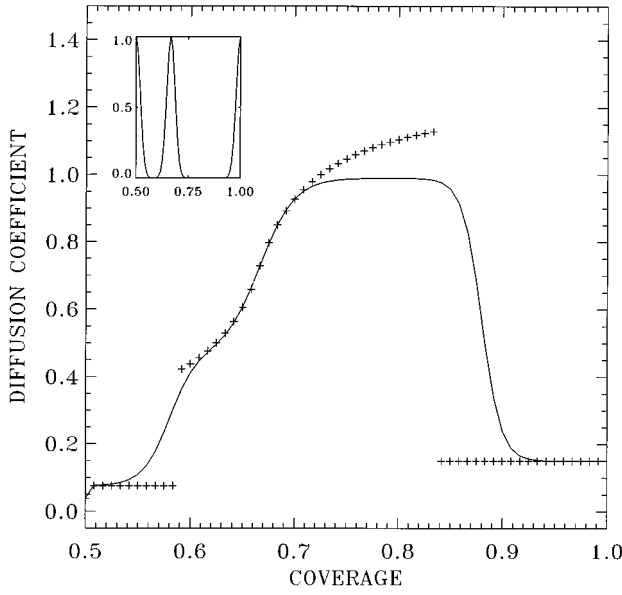
FIG. 8. Chemical diffusion coefficient D_c versus coverage for $T=0.025$ eV. Crosses correspond to the D_c values calculated with phenomenological equations (13)–(19); the full curve corresponds to the $D_c(\theta)$ dependence, interpolated with the help of the weighting coefficient presented in the inset.

this procedure cannot avoid some arbitrariness, we keep it to a minimum by putting the weighting factor to zero wherever the theoretical formula for $D_c(\theta)$ is not valid. The general shape of the interpolated $D_c(\theta)$ reflects the expected general variations of the chemical diffusivity versus coverage. We see that this function monotonically increases in the region $1/2 < \theta < 2/3$ (corresponding to the decrease of the activation

energy E_{ac} which can be deduced from Fig. 1), while at higher coverages D_c start to decrease. The *high-temperature* behavior of D_c at high coverages is given in the kink-gas approach by the variation of kink mass. It can be also interpreted in terms of the Arrhenius formula $D_c = D_0 \exp(-E_{ac}/T)$. Generally, D_0 and E_{ac} change in a similar manner (the so-called *compensation effect*[1]). At high enough temperatures, the slow decrease of E_{ac} at $\theta > 2/3$ (see Fig. 1) leads only to a slow change of the exponential term of the Arrhenius formula. The fast drop of D_c must thus be attributed to the prefactor D_0.

Once D_c is known, the second step is to solve Eq. (21) with this D_c dependence and compare with the MD simulations. To deduce a local coverage from the MD atomic configuration at a given time t, we calculate the occupation numbers $n(i_x, i_y; t)$ (where $i_x = 1, \ldots, M_x$ and $i_y = 1, \ldots, M_y$) defined as the number of atoms in the given elementary cell (i_x, i_y). The results of the simulations for the 2D model ($M_x = 84$, $M_y = 60$, and $N = 3780$) are presented in Fig. 9. We started with an artificially prepared stepwise initial configuration: concentration $\theta = 1$ in the central region of the lattice (for $i_x = M_x/4 + 1, \ldots, 3M_x/4$) and $\theta = 0.5$ outside this region. The system is then allowed to evolve according to the Langevin equations (9). The concentration profile $\theta(i_x, t_n) = \sum_{i_y=1}^{M_y} n(i_x, i_y; t_n)/M_y$ is recorded at times $t_n = n t_0$. The simulation was repeated five times in order to average the profiles and decrease statistical fluctuations. The simulation profiles for different times are shown in Fig. 9 with symbols. They have a flatter section in the middle of the studied coverage interval, corresponding to the coverage region with enhanced diffusivity. Moreover, in the same figure, we plot with solid lines the theoretical profiles obtained from
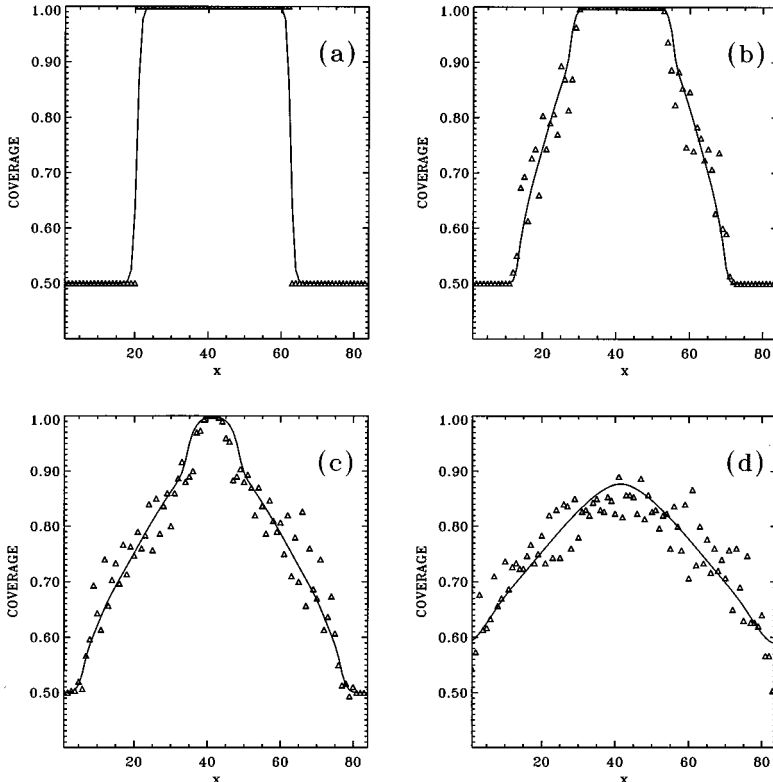

FIG. 9. Evolution of the coverage profile versus time: $t=0$ (a), $t=190$ (b), $t=763$ (c), and $t=1715$ (d). The triangles correspond to the simulation of the 2D model with $M_x = 84$, $M_y = 60$, and $N = 3780$ at room temperature $T = 0.025$ eV, and the full curves are the solution of the diffusion equation (21). The coordinate x is indicated in lattice units a_{sx}.

the numerical solution of the diffusion equation (21) with $D_c(\theta)$ plotted in Fig. 8. The data presented in Fig. 9 show that the theoretical and simulation results are in very good agreement, which validates the phenomenological approach used for determining the diffusion coefficient.

VI. DISCUSSION IN RELATION TO EXPERIMENTS

It is important to examine the applicability of the theoretical results to real physical systems such as atomic layers adsorbed on crystal surfaces. Although experiments cannot provide results as detailed as the numerical simulations, a comparison is possible. Our model is oversimplified to describe quantitatively a real adsystem — although we chose some model parameters close to those available for the K-W(112) adsystem — mainly because the interatomic interaction in real adsystems is much more complicated than the exponential interaction used in the present work.[20] In the case of adsorption on isotropic surfaces, diffusion is affected by the formation of domain walls, especially when the interatomic interaction is long range. Our results are more suitable to describe highly anisotropic surfaces for which the interaction between neighboring channels is sufficiently weak to reduce the role of two-dimensional domain walls. We obtain a qualitative agreement with experiments on diffusion of atoms adsorbed on highly anisotropic furrowed surfaces.

There are very few experimental data on the variation versus coverage of the diffusion coefficient for atoms adsorbed on highly anisotropic (furrowed) surfaces. Some data have been obtained using the field emission fluctuations method[36] for K-W(112) and the diffusivity was found to increase strongly in the region of the commensurate-incommensurate transition: this was interpreted in terms of fast diffusion of *solitons*.[36]

Detailed dependencies $D_c(\theta)$ and $E_{ac}(\theta)$ in the wide coverage interval $[0.05,1.5]$ are available[23] for Li-Mo(112), where the interaction between Li adatoms on Mo(112) is long range and anisotropic. Besides the short-range forces, the interaction between the adatoms includes also a dipole-dipole repulsion and an oscillating part due to substrate-mediated electron exchange.[20] This is responsible for the existence of peculiar chainlike structures $p(1\times4)$ and $p(1\times2)$, formed by first-order transitions, for coverages $\theta<0.5$.[37] In this range of θ, the diffusivity D_c was found to depend only weakly on coverage. At higher coverages $\theta>0.5$, the repulsion between Li adatoms starts to play a larger role. This results first in the formation of one-dimensional incoherent structures at $\theta\approx2/3$, and then the adlayer exhibits a one-dimensional compression along the direction of furrows.[37] In this coverage range, $D_c(\theta)$ was found to increase strongly and monotonically with coverage at low temperatures. The sharpest increases of diffusivity at low temperatures ($T<250$ K) appear for the commensurate coverages $\theta=2/3$ and $\theta=1$. This behavior of D_c coincides qualitatively with the predictions of the kink-gas approach[6] and our numerical simulations. Moreover, the activation energy E_{ac} for chemical diffusion, obtained in Ref. 23 from the slopes of Arrhenius plots of D_c, exhibits a monotonic decrease as coverage increases (except for small maxima at coverages slightly above the commensurate values $\theta=2/3$

and $\theta=1$), which is close to the behavior of ε_{PN} in Fig. 1. It is also interesting to notice that if $D_c(\theta)$ is plotted at temperatures higher than 300 K from the values of the prefactor D_0 and activation energy E_{ac} measured in Ref. 23, it shows a nonmonotonic behavior with a minimum around $\theta=1$, which is very similar to the behavior of D_c at $T=300$ K in the two-dimensional FK model considered here (see Sec. V).

Finally, preliminary results of the diffusion study in Sr-Mo(112) system[23] have demonstrated that diffusivity increases sharply at coverage $\theta\approx0.5$ which correspond to the commensurate (4×2) structure of strontium atoms (while at higher coverages Sr atoms form incommensurate structures). One may speculate that this enhanced diffusivity is provided by the fast kink diffusion.

VII. CONCLUSION

The aim of this paper was to check the predictions of the kink-gas approach with the help of molecular dynamics simulations. The validity of the kink-gas approach ought to be questioned because it is based on one-dimensional models while real adsystems are 2D (or even 3D taking into account the possible motion of adatoms orthogonal to the surface).

First, we compared the kink-gas approach [Eqs. (13)–(19)] and high-temperature formula (20) for mobility B and chemical diffusivity $D_c=k_BTB/\chi$ with the results of our simulation of FK models with transverse degrees of freedom. We have found only a *qualitative* agreement between the $B(\theta)$ dependencies obtained in MD simulation of 2D and 1D models with transverse degrees of freedom and those predicted by the kink-gas approach. In Sec. IV, we showed that the mobility B is strongly reduced when additional transverse dimensions are involved in the system. A *quantitative* estimation of B using Eqs. (13)–(19) shows that the kink-gas approach overestimates the mobility significantly unless we artificially introduce a higher effective friction η_{eff}. This can be understood because some part of the energy brought into the system by the external force is absorbed by extra degrees of freedom. For example, in the simplest case of harmonically interacting atoms at high temperatures, the mobility has to be renormalized by a factor 1/3 (i.e., $\eta_{eff}=3\eta$) due to the presence of two additional degrees of freedom, since the energy is redistributed uniformly ($\sim k_BT/2$) between all three degrees of freedom. But in our case, where interaction between atoms is anharmonic and mobility is investigated at low temperatures, a reliable determination of the effective friction η_{eff} is not possible.

By contrast, the study of chemical diffusion (Sec. V) demonstrates *qualitative* and *quantitative* agreement between MD simulation data and the kink-gas approach. The reason is that in the case of thermal diffusion, the chemical diffusion coefficient $D_c=k_BTB/\chi$ does not change with additional degrees of freedom since the "external force" is provided by the thermal energy of the system and is proportional to the gradient of the chemical potential μ. As the Fick law (2) may be rewritten as $J=\rho B\nabla\mu=\rho B(\partial\mu/\partial\rho)\nabla\rho=k_BTB/\chi\nabla\rho$, where $\chi\equiv(\partial\ln\rho)/(\partial\mu/k_BT)$, it is clear that an additional transverse dimension to the system leads simultaneously to an increase of free energy and chemical potential μ. In other words, the decrease of the system's mobility due to an extra transverse dimension of the system is compen-

sated by a corresponding decrease of the susceptibility χ of the system, so that D_c remains approximately the same.

Our results allow us to conclude that the phenomenological kink-gas approach provides a good qualitative explanation not only for molecular dynamics simulation data of mobility and diffusivity versus atomic coverage in the generalized 2D Frenkel Kontorova model, but also for some experimental results on the coverage dependence of surface diffusion. Obviously, for a better description of real adsorption systems, the Frenkel-Kontorova model should take into account long-range, anisotropic, realistic interatomic interac-

tions and the presence of surface defects.

---

[*] Electronic address: tdauxois@physique.ens-lyon.fr

[1] A. G. Naumovets and Yu. S. Vedula, Surf. Sci. Rep. **4**, 365 (1985); R. Gomer, Rep. Prog. Phys. **53**, 917 (1990).

[2] C. Uebing and R. Gomer, J. Chem Phys. **95**, 7626 (1991); **95**, 7636 (1991); **95**, 7641 (1991); **95**, 7648 (1991); M. Tringides and R. Gomer, Surf. Sci. **265**, 283 (1992).

[3] W. Dieterich and I. Peschel, Physica A **95**, 208 (1979).

[4] R. W. Holloway and M. J. Gillan, Solid State Commun. **52**, 705 (1984); M. J. Gillan and R. W. Holloway, J. Phys. C **18**, 4903 (1985).

[5] M. J. Gillan and R. W. Holloway, J. Phys. C **18**, 5705 (1985).

[6] O. M. Braun and Yu. S. Kivshar, Phys. Rev. B **50**, 13 388 (1994).

[7] Ya. Frenkel and T. Kontorova, Phys. Z. Sowietunion **13**, 1 (1938).

[8] H. R. Paneth, Phys. Rev. **80**, 708 (1950).

[9] I. F. Lyuksyutov, A. G. Naumovets, and V. L. Pokrovsky, *Two-Dimensional Crystals* (Naukova Dumka, Kiev, 1983; Academic, Boston, 1992).

[10] J. B. Boyce and B. A. Huberman, Phys. Rep. **51**, 189 (1979).

[11] St. Pnevmatikos, A. V. Savin, A. V. Zolotaryuk, Yu. S. Kivshar, and M. J. Velgakis, Phys. Rev. A **43**, 5518 (1991).

[12] T. Munakata and A. Tsurui, Z. Phys. B **34**, 203 (1979).

[13] T. Geisel, Phys. Rev. B **20**, 4294 (1979).

[14] A. R. Bishop, W. Dieterich, and I. Peschel, Z. Phys. B **33**, 187 (1979).

[15] O. M. Braun, Yu. S. Kivshar, and I. I. Zelenskaya, Phys. Rev. B **41**, 7118 (1990).

[16] A. Milchev and I. Markov, Surf. Sci. **136**, 503 (1984); **136**, 519 (1984); **145**, 313 (1984); **156**, 392 (1985).

[17] M. Peyrard and M. Remoissenet, Phys. Rev. B **26**, 2886 (1982).

[18] B. Bayat and H.-W. Wassmuth, Surf. Sci. **133**, 1 (1983).

[19] O. M. Braun and E. A. Pashitsky, Poverkhn. Fiz. Himiya Mechan. (USSR) No. 7, 49 (1984) [Phys. Chem. Mech. Surf. (U.K.) **3**, 1989 (1985)].

[20] O. M. Braun and V. K. Medvedev, Usp. Fiz. Nauk **157**, 631 (1989) [Sov. Phys. Usp. **32**, 328 (1989)].

[21] O. M. Braun, A. I. Volokitin, and V. P. Zhdanov, Usp. Fiz. Nauk **158**, 421 (1989) [Sov. Phys. Usp. **32**, 605 (1989)].

[22] A. Zangwill, *Physics at Surfaces* (Cambridge University Press, Cambridge, England, 1988).

[23] A. T. Loburets, A. G. Naumovets, M. V. Paliy, N. B. Senenko, and Yu. S. Vedula, Prog. Surf. Sci. **48**, 59 (1995).

[24] O. M. Braun, T. Dauxois, and M. Peyrard, preceding paper, Phys. Rev. B. **54**, 313 (1996).

[25] O. M. Braun, O. A. Chubykalo, and T. P. Valkering (unpublished).

[26] O. M. Braun and M. Peyrard, Phys. Rev. B **51**, 17 158 (1995).

[27] O. M. Braun and M. Peyrard, Phys. Rev. E **51**, 4999 (1995).

[28] A. Seeger and P. Schiller, in *Physical Acoustics*, edited by W. P. Mason (Academic, New York, 1966), Vol. IIIA, p. 361.

[29] B. V. Petukov and V. L. Pokrovsky, Sov. Phys. JETP **36**, 336 (1973).

[30] J. F. Currie, J. A. Krumhansl, A. R. Bishop, and S. E. Trullinger, Phys. Rev. B **22**, 477 (1980).

[31] M. Büttiker and R. Landauer, Phys. Rev. A **23**, 1397 (1981).

[32] F. Marchesoni, Ber. Bunsenges. Phys. Chem. **95**, 353 (1991).

[33] M. Remoissenet, Solid State Commun. **27**, 681 (1978).

[34] D. J. Bergman *et al.*, Phys. Rev. A **27**, 3345 (1983).

[35] F. Marchesoni, Phys. Lett. A **115**, 29 (1986).

[36] R. Blaszchyszyn and Ch. Kleint, Surf. Sci. **171**, 715 (1986); J. Beben, Ch. Kleint, and A. Pawelek, *ibid.* **213**, 451 (1989); J. Beben, Ch. Kleint, and R. Meclewski, Z. Phys. **69**, 319 (1987).

[37] M. S. Gupalo, V. K. Medvedev, B. M. Paliukh, and T. P. Smereka, Sov. Phys. Solid State **21**, 568 (1979).